Journal of Physical Sciences, Vol. 22, 2017, 137-150
ISSN: 2350-0352 (print), www.vidyasagar.ac.in/journal
Published on 25 December 2017

Perspective of Distortion and Vulnerability in Structure by Using the CdS-ZnS Composite Approach in Rietveld Refinement

Nishant T. Tayade[1], Sachin Dhawankar[2] and P. R. Arjuwadkar[3]

[1,3] Department of Physics, Institute of Science, R.T. Road, Civil Line
Nagpur (M.S.) – 440001, India
[2]Department of Physics, Chhatrapati Shivaji Institute of Technology
Durg – 491001 (C.G), Email: nishanttayade@rediffmail.com
Received 3 October 2017; accepted 12 November2017

ABSTRACT

ZnS-CdS composite structure solid film was prepared by spry-pyrolysis technique. Structural analysis conducted using Rietveld refinement of PXRD pattern and FFT. From this, unit cells of the three phases with ZnSW(8H) (dominant) and others hexagonal and cubic CdS have been solved. Present work has done the tetrahedron analysis to study the distorted tetrahedrons. The limitations of highly distorted hexagonal phases innovatively examined in this paper, which has implemented an idea of the possible direction of tetrahedral distortions. From overall analysis, the structural perspective of spray pyrolysis made film has discussed in this paper along with SEM and UV-VIS data. In this work, the consideration of the assembly of ZnS-CdS composite is found practically very significant. It gives direct sub-structural contribution to understand the bigger composite structure with the details of tetrahedral level minute distortions which will be responsible for the single phase material of ternary-compound and showing its optical properties with semiconductor nature.

Keywords: ZnCdS film, CdS-ZnS composite, Rietveld analysis, tetrahedron distortion, structural vulnerability.

1. Introduction

Zinc sulphide and Cadmium sulphide belongs to II – VI compound group. Zinc sulphide and Cadmium sulphide are semiconductor material with an optical energy band of 3.5eV and 2.5eV respectively and with n- type conductivity and electrical resistivity of the order of $10^4 – 10^5$ Ω cm [1-3]. Zinc cadmium sulphide (*ZnCdS*), Halff-half composition of CdS and ZnS, is a ternary II-VI compound semiconducting material having direct band gap. The band gap varies from 2.5 to 3.5eV [4]. Several method for depositing ZnCdS and CdZnS thin films are available in the literature such as chemical bath deposition [5], vacuum co-evaporation technique [6], spray pyrolysis [7] Fig.1, electro deposition [8],

successive ionic layer adsorption and reaction (SILAR) [9] etc. The X-ray diffraction (XRD) patterns of CdS films after Zn doping have shown a more disordered nature and consisting of reflections from $Zn_{0.049}Cd_{0.951}S$ as well as CdS greenockite (hexagonal) and hawleyite (cubic) phases [10]. In those, the cut-off wavelength was modified after Zn doping and the film exhibits promising characteristics for application in solar cell and photo detector structures. Both the hexagonal and cubic reflections in a XRD were observed in a nanosheet for different Zn and Cd ion concentrations [11]. Using a dip-coating, researcher found cubic structure for $Zn_{1-x}Cd_xS$ where x=0.1 shows three peaks with great broadening and appeared as a single curved peak [12]. In the field of H_2 evolution by water splitting using ZnCdS as a catalyst, the cubic and hexagonal ZnCdS structural behaviour has been found in literature where XRD has clearly shown that some more peaks are appearing in a profile for cubic to hexagonal change [13]. As usually the convolution of peaks occurs in small nanosize structures which hides some important peaks by which proper analysis get affected.

In the present work, an idea is that the CdS and ZnS phases can be more responsible to form the $Zn_{0.5}Cd_{0.5}S$ with certain degree of distortion and act as the CdS/ZnS super lattice semiconductor. All structural phases therefore, can be contributing their energy bands for the resultant energy band gap. If this is true then the fitting by XRD profile for all phases can provide more precise details of real structural perspective. It has been done in this paper using the Rietveld refinement method which further inspects the distortion and the limit of vulnerability of the unit cell.

2. Materials and methods

2.1. Synthesis

An aqueous solution of Cadmium chloride ($CdCl_2$), Zinc acetate [$(CH_3COO)_2$ $Zn.2H_2OH_2O$] and Thiourea (CH_4N_2S) are used as a source. Cadmium chloride (0.1 N) and Zinc acetate (0.1N) solutions were prepared with 100ml and Thiourea (0.1N) solution was prepared with 200ml of double distilled water and each solution stirrer for 5 hours using electronic stirrer. These were mixed to form ternary compound solution which was stirred for 2 hours. After cleaning process the glass substrate was weighed before deposition using an electronic unipan microbalance of accuracy 10^{-4} gm. The clean dielectric (glass) substrate is arranged on the hot plate of spray pyrolysis setup with a nozzle distance of 30 cm and flow rate of precursor 15cc/min at temperature 390^{o}C. Deposited ZnCdS thin film dielectric substrate was weighed and studies for thickness using gravimetric method.

2.2. Characterization

Thickness was obtained from the Michelson-Morley Interferometer along with gravimetric analysis. In an XRD experiment, the data (using Bruker AXS D8 Advance) have been obtained for 1.5406Å Cu-Ka radiation with a step of 0.02 for the range 10 to 80 degrees. A profile pattern data in the UXD raw format and the irf data were collected for analysis. Optical spectrometric experiment was carried out on Elico SL159 spectrophotometer for the range of wavelength from 380 to

1000 nm with a step of 1nm. The weighting method experiment used to determine the thickness of deposited film. The morphology has been obtained by SEM (JEOL Model JSM - 6390LV) for 10,000 times magnification at 20KV.

2.3. Methods of analysis

The Fullprof [14] (collection of programs) tool for Rietveld refinement [15] has been used for the finding the structural solution for the sample. The least square fitting with pseudo Voight function was used for full profile fitting. Background and the *dat* file were first generated from raw data using winplotter [16]. Other programs [17] were used also at this stage. Using the cif files available at AMCSD [18][19] and COD-Inorganic databases, pcr file was made and checked it for various combinations of possible phase. The cif, ins, inp and other very essential files along with prf file were created for the present study.

3. Results and discussion

3.1. Film and its morphology

Thickness of the film is found 0.273µm and truncated on fourth decimal. Morphology is found similar to the reported works [10]. The SEM micrograph with 1µm scale (Fig.1) shows the grain formation of different size over the surface with different size (two are shown in second row of Fig.1). It has been studied for size distribution from the different parts. Sizes of the particles bounded in a film are ranging from 62.56nm to 143.30 nm. Shape has observed spherical. Mean size is found as 98.15±17.13 nm. Surface is not very uniform. The cluster of ZnS and CdS composites assembly must be dominant. This may be related to structural disorder. Formation of bigger particles from the isotropic stacking assembly of crystallites for all phases can't be denied. It can be the collection of all phases' crystallites particles or its groups.

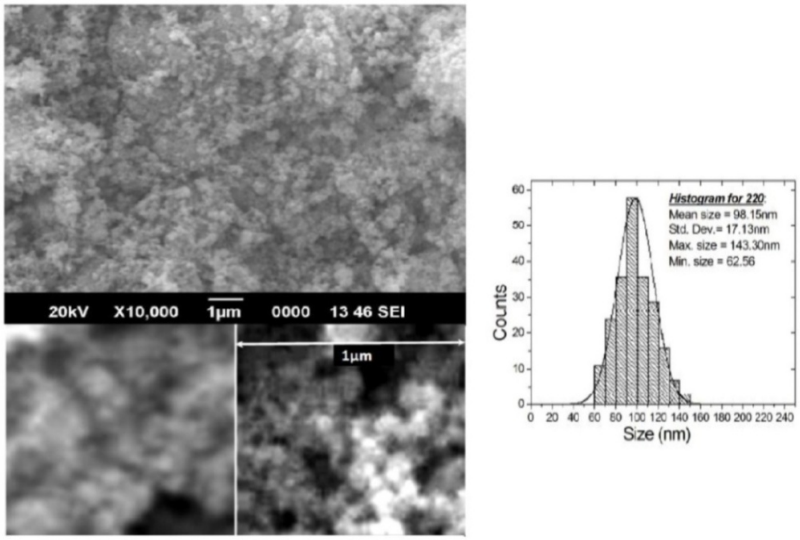

Figure 1: (a) SEM microphotograph of small scrubbed sample with Histogram of selected part for 1µm scale portion.

3.2. Optical study

An optical energy band gap for the direct allowed transition has been determined from the extrapolation on x-axis of a plot (method is discussed in [2][3]) as shown in Fig.2(b). It was found 2.8eV, which has a close agreement to the literatures reviewed in this paper [1-13] and indicated the semiconducting nature but slightly more than 2.5eV. The film absorbs more ultra-violet light than visible (see Fig.2 (a)) and its absorption peak is observed in a violet region. Film is found optically non-linear in ultra-violet region. The narrow peak in UV and shift indicate the presence of the quantum confinement effect. According to the literature [1-4], such materials possess n-type conductivity. Film is transparent to the visible light in a linear nature.

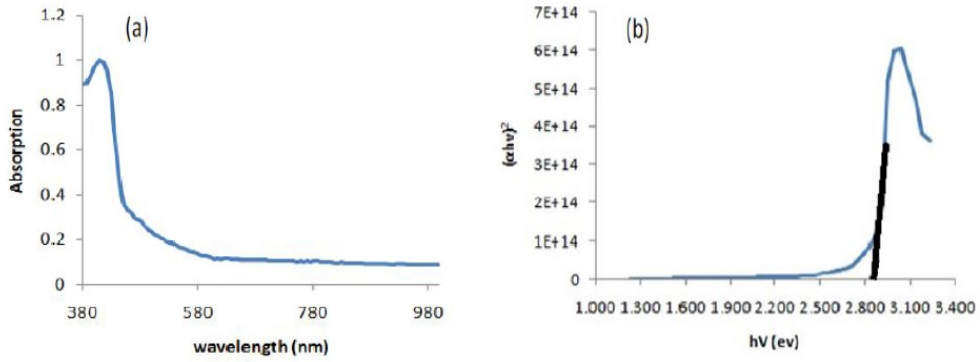

Figure 2: (a) Absorption plot and (b) Direct energy band gap determination

3.3. Rietveld analysis, phases and structure

The PXRD data (red scattering marker in Fig.3) represents the success of the formation of the film of good crystalinity and nanosize grains. Rietveld refinement of XRD pattern file has been plotted in Fig.3. A black colour is a calculated refined fit over a red colour observed data of the pattern shows that a profile-fit is good and the R-factors given in plot have confirmed its success of finding a solution. For the last convergence R-Factor [22] found 5.02 with 1.77 Chi^2 value. Other conventional and global factors are given in Fig.3. For the combinations of different phases of ZnS and CdS, few attempts were made to check for better matching of peak profiles. During the matching, wrutzite-8H [23] of ZnS-H in COD-Inorg-96-900-0087 has fitted best along with CdS-C in COD-inorg-96-900-8840)[24] and CdS-H in COD-inorg-96-101-1055) [25] (C for cubic and H for hexagonal phases). Indexing has confirmed these phases' formation, which were identified as phase1- hexagonal ZnS Wurtzite-8H, phase2-CdS cubic and phase3 hexagonal CdS which has been provided in a supplementary sheet for all indexed hkl values. The reflection with 100% for CdS-H indexed (101) (d=3.16, 2θ=28.254) matched with JCPDS-41-1049. The reflection with 100% for CdS-C indexed (111) (d=3.33, 2θ=26.736^o) close to JCPDS-80-0019 but the'd' has shifted slightly toward shorter value.

The lattice parameters with crystal structure of extracting phases have been given in a Table1. Quantitative analysis has found ZnS to be abundant (52.4%)

while CdS phases (cubic 26.0%, hexagonal=21.4%) are less in quantity in a sample. Very small quantity of the cubic ZnS might be possible, but due to comparison with others quantities and higher background and uncertainty, it has been observed insignificant.

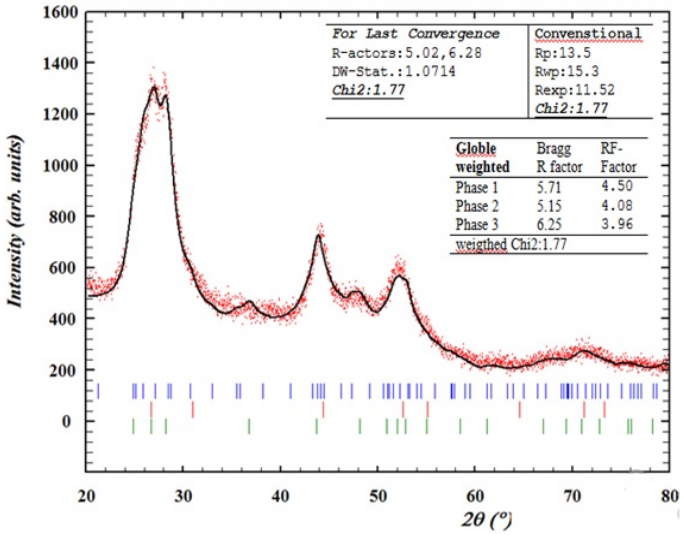

Figure 3: Rietveld refinement of PXRD data pattern; calculated pattern in black curve over observe pattern in red colour data

Phase	Chemical Compound	*Structure and symmetry*		*Cell Parameter*		Volume ($Å^3$)
		Crystal structure	SPGR H-M/Hall	a, c (Å)	α/β, ϒ (deg)	
Phase1	ZnS	Wurtzite-8H Hexagonal	P 63 m c P 6c -2c	4.129 25.04	90, 120.	369.7
Phase2	CdS	Hawleyite Cubic	F -4 3 m F -4 2 3	5.771 5.771	90, 90.	192.1
Phase3	CdS	α-Greenockite Hexagonal	P 63 m c P 6c -2c	4.137 6.671	90, 120.	98.85

Table 1: Crystal structure of Phases

3.4. FFT analysis for structure

A Fast Fourier Transform (FFT) subroutine in a GFourier tool is used to accelerate the calculation of the scattering density inside the unit cell of a crystal using the expression [20].

$$\rho(r) = \frac{1}{V}\sum_H F(H)\, e^{-2\pi i(H.r)},$$

where, V is volume of the unit cell, H is a reciprocal lattice vector, r is a vector position inside the unit cell, and F(H) are complex Fourier coefficients. The unit of ρ(r) is electron unit per $Å^3$. The data in the form of contour plots and map were

retrieved. Density map has plotted against the setting limit 0 to 1 for x/a, y/b and z/c. Analysis for Phase1 is given here in Fig.4 which shows the density plot in 3D for x/a and y/b. Corresponding 2D counter map selected for analysis after study which are shown in Fig.5(a). First row is the slices of the x/a (vertically) versus y/b (horizontally) contour map for the contour plotted for the z/c (horizontally) versus x/a (vertically). Also the variation in scattering density is represented increasing as blue-red-yellow sequence. The x/a versus y/b plot was made for all sums, however the z/a versus x/a for positive sum only. By recognizing and connecting the entire possible dense contour with each other, an initial idea has been developed. It has been finalized in Fig.5(b) that how would be the structure for Phase1 is visualized normal to b-direction (outward to plane of the paper) for 3D visualization of unit cell of ZnS-H (W-8) is shown in Fig.6 for extracted pattern of phase1 in a refined data.

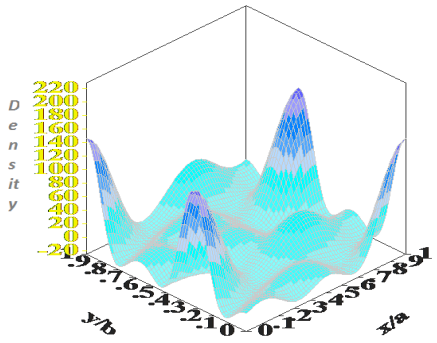

Figure 4: FFT 3D map of scattering density inside the crystal in plane (x/a, y/b) at z/c=0.

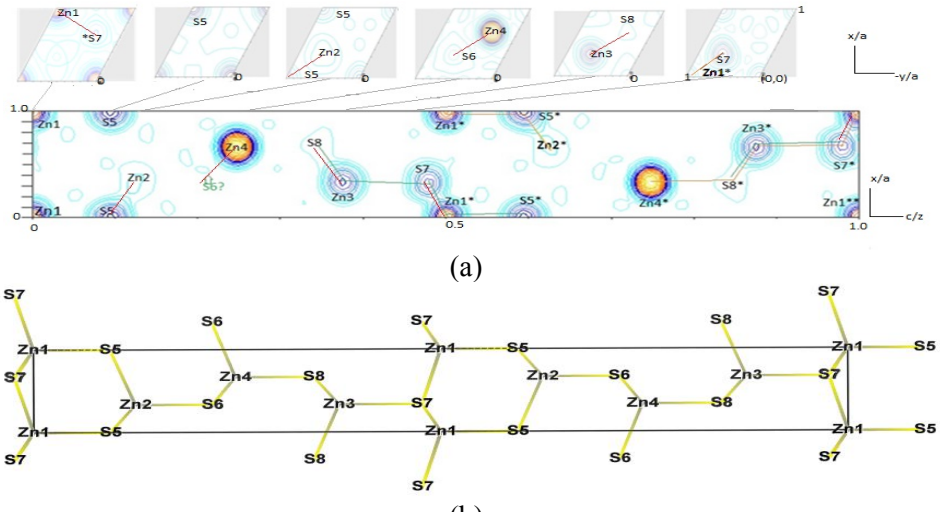

(a)

(b)

Figure 5: FFT analysis (a) charge density of scattering inside the unit cell for phase1 and (b) formation of unit cell structure

Same procedure of FFT has been employed to analyze other phases. All unit cells' 3D visualizations have directly shown in Fig.6 with its deconvulation extracted patterns. All these structures' visualizations were obtained by the VESTA program using the crystallographic information file (cif) created in the last cycle of the Rietveld refinement and information of its positions, sites and symmetries given in Table2.

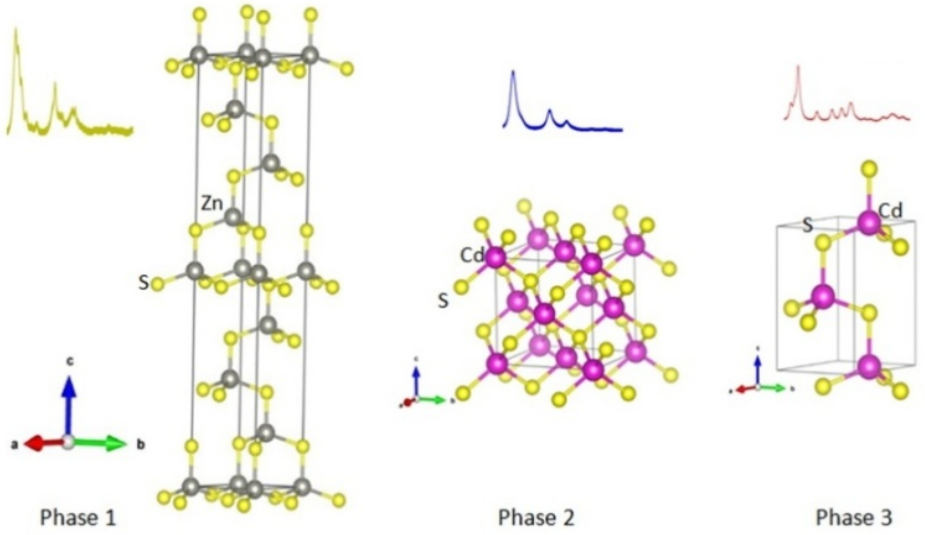

Figure 6: Extracted phase-patterns obtained after refinement and solved unit cells.

Phases	***Atoms***	**x**	**y**	**z**	***Site***	***Symmetry***
ZnS Phase1	Zn	0.00000	0.00000	0.00000	2a	3m
	3Zn	0.33333	0.66667	0.12500 0.37500 0.74770	2b	3m
	S	0.00000	0.00000	0.09400	2a	3m
	3S	0. 33333	0.66667	0.21900 0.47655 0.84400	2b	3m
Cubic CdS Phase2	Cd	0.00000	0.00000	0.00000	4a	-43m
	S	0.25000	0.25000	0.25000	4c	-43m
Hexagonal CdS Phase3	Cd	0.33333	0.66667	0.00000	2b	3m

Table 2: Positions of atoms in cell, sites and symmetries

3.5. Analysis of Tetragonal sub-structures

The bond lengths and angles were obtained by running CLF in Bond_Str program and by cif in VESTA and by FFT and are found very approximate. Details analysis about the bond lengths and angles corresponding to the concerned tetrahedral are summarized in Table3 and corresponding representation is illustrated in Fig.7. In phase2, it seems negligible distortion in tetrahedrons of cubic CdS. No one sample has an exact 109^o angle of (S-x-S) in tetrahedrons (where x is Zn or Cd). Only Phase2 has shown zero angle variance and zero bond length distortion indexes. These two parameters are positive and very small in Phase3. But in Phase1, all tetrahedral are distorted. Among all tetrahedral of Phase1, a bond angle variance in Z1-tetrahedron is very high i.e. 34.04 deg^2 and for the tetrahedron Z2, Z3 and Z4 remarkably high. Angles and average bond lengths are summarized in Table3. From all data, the distorted tetrahedron's sequence is found QZ1>Z4>Z2>Z3.

Tetrahedral Parameters		***Phase1*** *ZnS Tetrahedrons*				***Phase2*** *CdS*	***Phase3*** *CdS*
		Z1	**Z2**	**Z3**	**Z4**		
Average bond length (Å)		2.4299	2.4688	2.5161	2.4703	2.4987	2.5226
Polyhedral volume (Å^3)		7.2378	7.7030	8.1683	7.7030	8.0065	8.2381
Distortion index$_{(\text{bond length})}$		0.01568	0.0233	0.0052	0.0119	0.0000	0.0041
Quadratic elongation		1.0118	1.0024	1.0006	1.0031	1.0000	1.0001
Angle (deg):	∠*S-Xn-S*	103.84 114.47	108.03 110.87	110.87 108.03	112.03 106.77	109.47	109.25 109.25 109.70
	∠X_1-*S*-X_2	(Zn1-S-Zn3)=103.84, (Zn3-S-Zn4)=108.03 (Zn4-S-Zn2)=106.77, (Zn1-S-Zn2)=108.03				109.47	109.25
Bond angle variance (deg^2)		34.0433	2.4098	2.4097	8.2853	0.0000	0.0591
Eff. coordination num.		3.9452	3.8642	3.9950	3.9699	4.0000	3.9968

Table 3: Analysis of Tetragonal structures in all phases

All Z1 are placed at the end corners as well as at the centre (half of c) in the unit cell and hence more vulnerable. The sequence goes with vulnerability on the c-scale as Zn at (1)c and (1/2)c, Zn at (1/4)c and the (1/8)c (consider c is the maximum length of cell in c-direction and bracket ( ) is multiple of it). It should be natural and therefore predicted here for ZnS-CdS film sample. The effective coordination number is also found less than 4 except phase2. A study directed that the CdS are close to the identical structure but ZnS has variation in the hexagonal wurtzite-8H unit cell throughout the film.

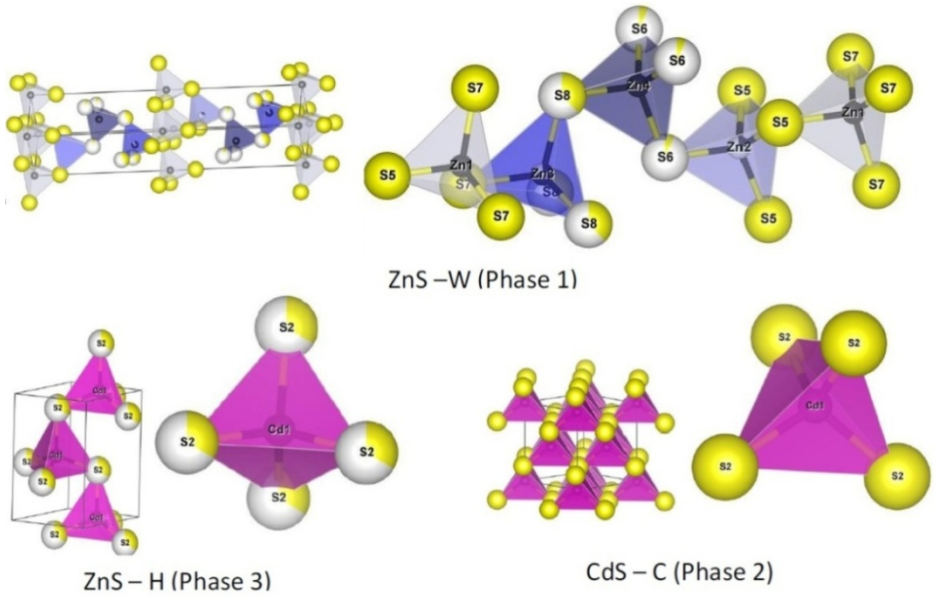

Figure 7: Tetragonal representation in the unit cells with its tetrahedral at its right side.

3.6. Microstructure investigation

Within a film, small crystallites have been formed. XRD pattern indicated the contribution of substrate background must be very small. The data obtained in the output file in Rietveld refinement keeping scale factor constant, detect atomic position fitting and fit on width parameters for integrated intensity is used for this analysis. An instrumental resolution function (irf) file was used before the execution of refinement.

Nanocrystallites particle size was estimated using the Debye Scherer formula:

$$D_{DS} = \frac{n\lambda}{\beta cos\theta},$$

where n=0.89 for spherical, λ is wavelength of Kα- Cu X ray, β is FWHM (full width of half maxima and θ is an angel concerned to Bragg reflection) for without consideration of strain factor [26]. The dislocation density (δ) (defined as the length of dislocation lines per unit volume) and the number of crystallites per unit area [27] in CdS-C is more than other phases shown in Table4 which are determine by –

$$\delta = \frac{1}{{D_{DS}}^2}$$

$$N = \frac{d}{{D_{DS}}^3}$$

where d is the inter-planner distance. Another method of Williamson Hall plot analysis [27] was also conducted to find size (D_{WH}) and strain (ε) using the equation:

$$\beta cos\theta = 4\varepsilon sin\theta + \frac{n\lambda}{D_{WH}}$$

which is used to plot a graph of β cosθ verses 4sinθ and fit it with regression for data as shown in Fig.8. The reciprocal of the intercept on the y-axis at x=0 gives the size and the slope of fit gives strain (see in Table4). Nanocrystallites sizes obtained for Phase1 and Phase2 from both methods are closer [27]. A cubic Phase2 has smallest crystallite size formation in a film with considerable negative strain. Phase3 has highest and positive strain and Phase1 is lowest and negative. Phase3 is more anisotropic in shape than the other. A cubic, hexagonal found retained in its structure, even with slight changes. But the both hexagonal (phases 1 and 2) have small variations in dimensions due to displacement of the atomic positions in the unit cells. The film is well oriented without stacking fault and the nanocrystallites cause the width of profile peaks interpreted from Fig.8.

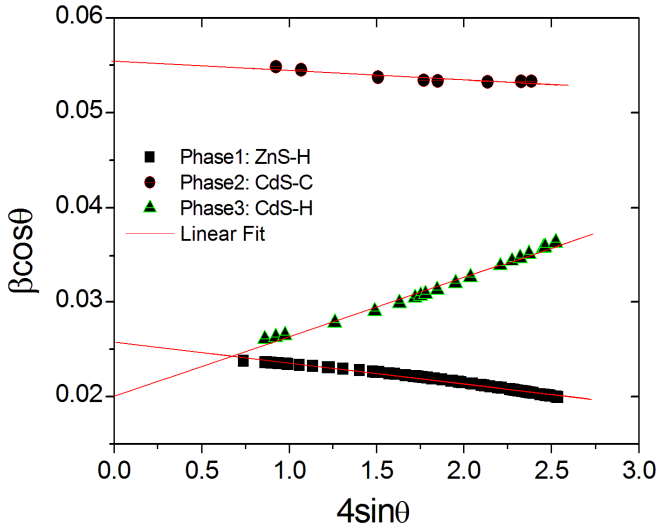

Figure 8: Williamson Hall plot analysis

Phases	***Debye Sherrer method***			***Williamson Hall Analysis***	
	Size (nm)	δ Lines m^{-2}	N m^{-2}	Size (nm)	Strain
Phase1: ZnS-H	5.88	2.89×10^{16}	1.69×10^{16}	5.38	-6.91×10^{-05}
Phase2: CdS-C	2.53	1.57×10^{17}	2.06×10^{17}	2.49	-3.19×10^{-04}
Phase3: CdS-H	5.23	3.65×10^{16}	2.20×10^{16}	6.92	$+3.12\times10^{-04}$

H-Hexagonal, C-cubic

Table 4: Microstructure parameters

3.7. Limit of Structural vulnerability due to refinement and correction

To check the limit of distorted tetragonal with highly carefully handling of refining parameter UVW along with positions (x, y and z) and occupancy, the Rietveld refinement has been done to reduce Chi^2 value and Braggs R-factor. The unit cells have shown totally spoiled with its original structure other than cubic CdS. Their unit cells are illustrated in Fig.9 for the Chi^2=1.31, R=4.17 5.39 R_{exp}=4.12, DW-Stat=1.49 and conventional Rietveld R-factors R=11.69 R_w=13.53, R_{exp}11.82 and global Bragg's R-factor/RF-factor for Phase1 are 1.96/1.78, for Phase2 1.15/1.34 and for Phase3 2.16/1.87 values. At this stage, the refinements became unstable before this cycle of fitting. Some time we got negative full width, some time parameters varied outside and sometime convergence failed. However, fitting of calculating pattern is very nice and improved compare to previously refinement. For 1.31 of GooF, the unit cells of ZnS-H and CdS-H are different from the previous (for Chi^2=1.77) in term of annihilation of tetrahedrons in ZnS and CdS-H. Tetrahedrons are the only polyhedrons which are existed in former stable refinement. There are no tetrahedrons exist in phase1 and in phase3 with 1.31GooF refinement. Instead, those, the polyhedrons of a coordinate numbers 3 are existed. There are two polyhedrons of volume 2.4785 $Å^3$ and average bond length 2.5880 Å with Zn2 atom in phase1 and with Cd in a phase3 two polyhedrons of volume 0.0970 $Å^3$ and average bond length 2.3900 Å.

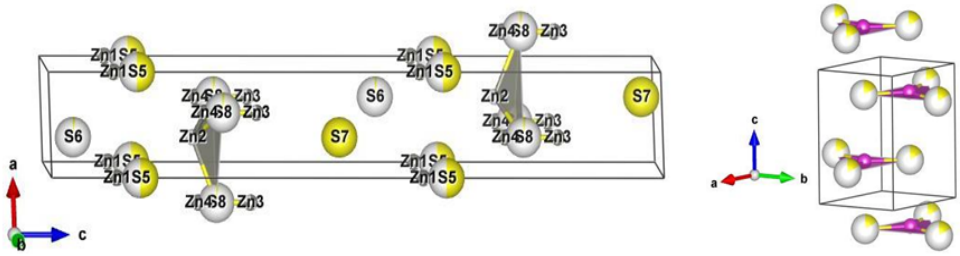

a,b=4.12928 c=25.03940;
V=369.745788 Å³

a,b=4.13900 c=6.68400
V= 99.164885 Å³

Figure 9: Limit of vulnerability due to distortion

A proposed structure for ZnS (shown in Fig.9) is not possible due to the positions and occupancy of Zn atoms has gone beyond the cell and for one phase has shown negative width. The problem with position is some extend possible to occur with Cd atoms in phase3 but the structure can be considered. Therefore, it is confirmed, our previous refinement gave trustworthy solution (Fig.6 and Fig.7) to the structure, but latter study gave new direction to think about structural vulnerability. A new idea to focus is the transformation from the previous tetrahedron cell of coordinate number 4 to coordinate number 3 by keeping cell parameter slightly changed. This idea can provide space to insert other phases'

atom. It could be possible if coordinate number is near to 4, As it varies from 4 to 3 then distortion in tetrahedron increases in term of bond length, angle variance or change in inner perspective of structure. In all phases, all surfaces of microstructures are found best to pack all phases over one another's surfaces and this process of packing is well ordered and bounded very tightly.

4. Conclusions

A synthesized film is applicable to make UV stopper, windows, opto-electronics semiconductor devices etc. From overall study, the structural perspective of spray pyrolysis made films must possess composite structures of CdS and ZnS for ZnCdS formation (for Cd+Zn=1 and S=1). Alongside the direct phase identification of ZnCdS, the composites study of it gives accurate information which can be support to other properties which are precisely dependent on structure. Occupancy of S is less in ZnS than CdS compare to single phases indicated that all "S atoms" have been shared in all phases. In c direction, a chain structure of ZnS was surrounded by CdS-H and CdS-C phases. Attached phases form a well with a little disordered-surface film. CdS-H suffers strain due to CdS-C and ZnS-H pressure on it in which only CdS-C left un-disordered. The nanosize spherical shapes became dominant at micrometer scale to form film morphology which was confirmed by XRD and SEM. Rather than a stable fitting done at Chi^2=1.77, the refinement for Chi^2=1.31 has given an idea of the possible direction of tetrahedral distortions i.e. c-direction displacement of tetrahedron in hexagonal cells. This is new outcome which has reported that the deformations occur at the site of polyhedral centres.

Acknowledgements

Authors of this paper acknowledge the support of STIC-SAIF, Cochin University of Science & Technology Cochin for the XRD and SEM characterization. We are very thankful to the authors of all codes in Fullprof and VESTA tools and their software developers and concerned Institution who have developed it with the great effort and provided it as an open source.

REFERENCES

1. H.M.Pathan and C.D.Lokande, Deposition of metal chalcogenide thin films by successive ionic layer absorption and reaction (SILAR) method, Bull. Mater. Sci., 27(2004) 85-111.
2. S.Dhawankar, A.K.Patil, J.S.Lad and B.M.Suryavanshi, Optical study of ZnS solid thin film prepared by spray prrolysis technique, Scholars Research Library, Archives of Physics Research, 4(3) (2013) 7-11.
3. S.Dhawankar and B.M.Suryavanshi, Characterization of cadmium sulphide (CdS) thin film deposited by spray pyrolysis technique, International Journal of Physical Research, 4(2) (2016) 58-61.
4. S.R.Kumar, S.Kumar, S.K.Sharma and D.Roy, Structure, Composition and Optical Properties of Non Aqueous Deposited ZnCdS Nanocrystalline Film, Materials Today: Proceedings, 2(2015) 4563-4568.

5. J.F.Mohammad and H.S.Al-jumaili, Sturstural and optical properties of Nanocrystalline $Zn_XCd_{1-X}S$ thin film deposited by chemical bath technique, International Journal of Application or Innovation in Engineering & management, 3(5) (2014) 204-210.
6. I.S.Naji, M.F.A.Alias and E.M.Naser, Impact of heat treatment on some physical properties of thin CdZnS, International Journal of Scientific Research, 2(3) (2013) 362-365.
7. D.J.Seo, Structal and optical properties of cdo films deposited by spray pyrolysis, Joural of the Korean Physical Society, 45(2004) 1575-1579.
8. A.A.AlBassan, Photocunductivity and defect level in $Zn_xCd_{1-x}Se$ (x=0.5,0.55) crystals, Solar Energy Mater. Sol. Cells, 57(1999) 323-329.
9. G.Laukaitish, S.Lindroos, S.Tamulevicius, M.Leskela and M.Rackitis, SILAR deposition of Cd x Zn 1-x S thin films, Appl. Surf. Sci., 161(3)(2000) 396-405.
10. P.J.Sebastian, ZnCdS films for solar cell and photo detector applications deposited by In Situ chemical doping of CdS with Zn, Advanced Functional Materials, 5(5) (1995) 269-275.
11. M.A.Mahdi, J.J.Hassan, S.S.Ng and Z.Hassan, High-Quality ZnCdS Nanosheets Prepared Using Solvothermal Synthesis, Journal of Nanoscience, 2013(2013) 1-6.
12. M.A.Rafea, A.A.M.Farag and N.Roushdy, Structural and optical characteristics of nano-sized structure of Zn0.5Cd0.5S thin films prepared by dip-coating method, Journal of Alloys and Compounds, 485(2009) 660.
13. C.C.Shen, Y.N.Liu, X.Zhou, H.L.Guo, Z.W.Zhao, K.Liang and A.W.Xu, Large improvement of visible-light photocatalytic H_2-evolution based on cocatalyst-free $Zn_{0.5}Cd_{0.5}S$ synthesized through a two-step process, Catal. Sci. Technol., 7(2017) 961-967.
14. J.R.Carvajal, A Program for Rietveld Refinement and Pattern Matching Analysis, Abstract of the Satellite Meeting on Powder Diffraction of the XV Congress of the IUCr, Toulouse, France, (1990) 127.
15. H.M.Rietveld, A profile refinement method for nuclear and magnetic structures, Journal of Applied Crystallography, 2(2)(1969) 65-71.
16. T.Roisnel and J.Rodríquez-Carvajal, WinPLOTR: A Windows Tool for Powder Diffraction Pattern Analysis,Materials Science Forum, 118(2001) 378-381.
17. J.R.Carvajal, Introduction to the Program FULLPROF: Refinement of Crystal and Magnetic Structures from Powder and Single Crystal Data, Laboratoire Léon Brillouin (CEA-CNRS), Saclay, France, 2001.
18. R.T.Downs and M.H.Wallace, The American Mineralogist Crystal Structure Database, American Mineralogist, 88(2003) 247-250.
19. http://rruff.geo.arizona.edu/AMS/amcsd.php accessed in May 2017.
20. J.González-Platas and J.R.Carvajal, GFourier: a Windows/Linux program to calculate and display Fourier maps. Program available within the FullProf Suite. (accessed in May 2017).
21. K.Momma and F.Izumi, VESTA: a three-dimensional visualization system for electronic and structural analysis, J. Appl. Crystallogr., 41(2008) 653-658.

22. B.H.Toby, R factors in Rietveld analysis: How good is good enough?, Powder Diffr., 21(2006) 67-70.
23. H.T.Evans and E.T.McKnight, New Wurtzite polytupes from Joplin Missouri, The American Mineralogist, 44(1959) 1210-1218.
24. F.Ulrich and W.Zachariasen, Ueber die Kristallstruktur des $-alpha- und $-beta CdS, sowiedes Wurtzits, Zeitschriftfuer Kristallographie, Kristallgeometrie, Kristallphysik, Kristallchemie, 62(1925) 260-273.
25. R.W.G. Wyckoff, New York Note: ZnS structure, sphalerite structure, Crystal Structures Second edition. Interscience Publishers, New York, 1(1963) 85-237.
26. B. D. Cullity and S. R. Stock, Principles of X-Ray Diffraction, Prentice Hall Inc. 2001.
27. V.D.Mote, Y.Purushottam and B.N.Dhole, Williamson-Hall analysis in estimation of lattice strain in nanometer-sized ZnO particles, J. Theoretical and Appl., 6(2012) 1-8.